Nanoscale Advances

ROYAL SOCIETY OF CHEMISTRY

PAPER

View Article Online
View Journal | View Issue

Cite this: *Nanoscale Adv.*, 2025, **7**, 2032

Graphene quantum dots as potential broad-spectrum antiviral agents†

Younghun Jung,‡[a] Jaehyeon Hwang,‡[a] Hyeonwoo Cho,‡[bc] Jeong Hyeon Yoon,[a] Jong-Hwan Lee,[b] Jaekwang Song,[b] Donghoon Kim,[d] Minchul Ahn,*[bc] Byung Hee Hong*[bc] and Dae-Hyuk Kweon*[a]

Received 25th October 2024
Accepted 24th January 2025

DOI: 10.1039/d4na00879k

rsc.li/nanoscale-advances

As pandemic viruses have become a threat to people, various treatments have been developed, including vaccines, neutralizing antibodies, and inhibitors. However, some mutations in the target envelope protein limit the efficiency of these treatments. Therefore, the development of broad-spectrum antiviral agents targeting mutation-free viral membranes is of considerable importance. Herein, we propose graphene quantum dots (GQDs) as broad-spectrum antiviral agents, wherein the amphiphilic properties of GQDs destroy the viral membranes, regardless of the type of viruses, including SARS-CoV-2 and influenza virus. We observed that GQDs suppress both viral infection and replication and demonstrated their low cytotoxicity in a cell line and a mouse model, revealing the potential of GQDs as a universal first-line treatment for various viral diseases.

1. Introduction

According to the World Health Organization (WHO), the coronavirus disease (COVID-19) has killed nearly 7 million people worldwide since its outbreak in 2019. COVID-19 caused by SARS-CoV-2 has caused a widespread threat and disruption worldwide, and it is now marking a chapter of a global pandemic in the history of humanity. Several viral outbreaks in the past 10 decades, including the Spanish flu of 1918, HIV, SARS, MERS, Ebola, ZIKA and the ongoing COVID-19, have been caused by highly fatal enveloped viruses.[1,2] In addition to pandemic diseases, such enveloped viruses are involved in human infectious diseases such as hepatitis, herpes, and smallpox.[3] Accordingly, efforts to develop vaccines are fast-paced around the world to counter these emerging viruses.

However, vaccine development is an expensive and time consuming process because it requires many efficacy and safety studies prior to clinical usage.[4,5] Additionally, the lack of understanding about newly emerging viruses often leads to difficulties in vaccine development. Furthermore, the repetitive re-emerging of viral mutants may periodically demand additional vaccine development as in the case of influenza vaccines. For instance, the E484K mutation of COVID-19, which was identified in South Africa and quickly spread in the UK, has become more resistant to vaccines owing to mutations in their spike protein.[6] Sole dependence on vaccine development is inadequate for rapid response to viral threats, as evidenced by COVID-19 and applicable to future emerging viral diseases.

Hence, the requirement for universal antiviral drugs have increased, and numerous studies have suggested potential broad-spectrum antiviral drugs based on peptides,[7–9] nanoparticles,[10–12] and small molecules.[13] To overcome the mutational vulnerability of viral proteins, these universal antiviral agents are designed to target the viral envelopes that are similar to cell membranes and disrupt them physically or chemically, thereby irreversibly inactivating the viruses.[14] In particular, graphene derivatives, such as modified graphene oxides, have been studied as antiviral agents owing to their high surface area, tunable chemical functionality, and amphiphilicity.[10,15–25] Although graphene derivatives show broad-spectrum antiviral activity, their cytotoxicity caused by their large sizes (100 nm to 1 μm) makes their development as actual drugs challenging. Herein, we propose a graphene quantum dot (GQD) with an average size of 5 nm as a novel antiviral agent that is effective against a wide range of viruses. GQDs are the smallest fragments of few-layered graphene nanoflakes that contain hydrophilic edges and hydrophobic basal planes. In recent years, GQDs with amphiphilic characteristics have been utilized to disaggregate protein fibrils like α-synucleins, β-amyloids, and cholesterol that cause degenerative brain diseases.[26,27] In addition, GQDs are less toxic than other large graphene derivatives because they are less than 20 nm in

[a]*Department of Integrative Biotechnology, College of Biotechnology and Bioengineering, Sungkyunkwan University, Suwon, 16419, Republic of Korea*
[b]*Department of Chemistry, Seoul National University, Seoul, 08826, Republic of Korea*
[c]*Graphene Research Center & Graphene Square Chemical Inc., Advanced Institute of Convergence Technology, Suwon, 16229, Republic of Korea*
[d]*Department of Pharmacology, Peripheral Neuropathy Research Center (PNRC), Dong-A University College of Medicine, Busan, 49201, Republic of Korea*

† Electronic supplementary information (ESI) available. See DOI: https://doi.org/10.1039/d4na00879k

‡ These authors contributed equally to this work.

size and can be quickly removed by renal clearance.[28–35] Moreover, in our previous study, we have confirmed that oral administration of GQDs do not affect the gut microbiota.[32] These ideal properties of amphiphilicity and low toxicity of GQDs indicate that they can be used as potential antiviral agents for regulating multiple strains of viruses.

The antiviral properties of GQDs against enveloped viruses have been reported to be enhanced by functionalization and doping.[36,37] However, to the best of our knowledge, no studies have been conducted using GQDs against non-enveloped viruses. Additionally, while studies have been conducted on enveloped viruses, there have been no reports optimizing antiviral efficacy through size control of GQDs for these viruses.

Herein, we synthesized GQDs through oxidative exfoliation and investigated their antiviral effects with respect to their sizes. On performing a series of *in vitro* experiments, we observed that GQDs significantly hindered the infection of several enveloped viruses, including SARS-CoV-2 and influenza virus, as well as the non-enveloped adenovirus. In addition, the virucidal effect by GQDs was visualized using bio-transmission electron microscopy (Bio-TEM). Notably, the complete disruption of the virus inhibited viral infection *in vivo*, and no symptoms and lethality were observed in mice. Thus, our results indicated that GQDs can potentially inhibit multiple viruses by disrupting the viral membranes *in vitro* and *in vivo*. Furthermore, the results from *in vitro* viral inhibition suggested their potential as a therapeutic and preventing agent.

2. Results and discussion

2.1 Preparation and characterizations of amphiphilic GQDs

To investigate the antiviral effects of GQDs, they were synthesized through the acidic oxidation of carbon black (Super P®), followed by filtration with a disc filter of 20 nm and dialysis with 1 kDa dialysis membrane for 3 days.[38,39] The dialyzed solution was lyophilized for 2 days to obtain a brownish-black powder with a yield of about ∼15%. The synthesized GQDs were characterized using TEM and dynamic light scattering (DLS) to confirm their morphological structure and size distribution, respectively. GQDs were observed to be monodispersed graphene fragments, and the average lateral size of GQDs was 2.36 ± 0.69 nm (Fig. 1a and b). Using the fast Fourier transform technique in the TEM image, the lattice space of GQDs was observed to be 0.24 nm, which was close to the *d* value of the graphene (100) plane.[40] The hydrodynamic size of GQDs was 5.08 ± 1.54 nm, and the zeta potential of GQDs was −10.6 ± 4.65 mV (Fig. S1†). We also performed XPS, FT-IR, Raman spectroscopy, and UV-vis spectroscopy to confirm the chemical structures of GQDs.

In the XPS spectra, we observed that the ratio of the C 1s to O 1s peak was about 0.8, which was similar to the C/O ratio obtained from elemental analysis (Fig. S2, Table S1†). C 1s peaks of GQDs were deconvoluted into three peaks at 284.5 eV, 286 eV, and 288 eV, which corresponded to the sp^2 carbon (C=C), alcohol group (C–O), and carbonyl group (O–C=O), respectively (Fig. 1c). In addition, FT-IR spectra demonstrated that GQDs contain aromatic rings (1650 cm^{-1} peaks, C=C stretching band) and diverse functional groups, such as carbonyl (1720 cm^{-1}, C=O stretching band) and hydroxyl groups (3400 cm^{-1}, O–H stretching) (Fig. 1d). The D band (1350 cm^{-1}) and G band (1580 cm^{-1}) corresponded to the characteristic Raman peak for graphene (Fig. S3†).[41] The UV-visible absorption band at 280 nm, which was related to the π–π* transition of conjugated C=C bonds, indicated that GQD samples had graphitic carbon cores.[42] As can be seen from the fluorescence image of GQDs at 365 nm excitation, GQDs exhibited yellow emission and emission peaks at ∼480 nm and ∼560 nm (Fig. S4†). From the above-mentioned results, we confirmed that GQDs were composed of a sp^2 carbon core and diverse functional groups, including oxygen, indicating that GQDs are amphiphilic agents.

2.2 Virucidal mode of action of GQDs on a viral envelope

We hypothesised that GQDs would perform a virucidal effect on a viral envelope through the amphipathicity obtained from the hydrophobic plane and hydrophilic edge of the graphene structure. To identify disruption of virions by GQDs, we assessed DLS, which enabled measuring the hydrodynamic size change of viruses on treatment with GQD (Fig. 2a). When treated with 0.1 and 1 mg mL^{-1} of GQDs, virus peaks in the DLS profile disappeared, indicating the complete disruption of the virus. At a lower concentration (0.01 mg mL^{-1}), intact PR8 viruses were still measured, indicating that a threshold amount of GQDs is required for viral disruption.

We performed TEM to verify disruption of the virus membrane by GQDs (Fig. 2b and c). After excess incubation in the presence of 0.05 mg mL^{-1} GQDs, most virions in the TEM image with a low magnitude disappeared (Fig. 2b). At short incubation time of less than 2 h at room temperature (Fig. 2c), partial disruption of the viral envelope was observed (Fig. 2c, right), whereas no disruption was observed until 1 h of incubation (Fig. 2c, left and center). These results presented the stepwise destruction of the influenza virus from intact virions to completely demolished debris.

2.3 Broad-spectrum antiviral activity against influenza virus and SARS-CoV-2

Prior to determining the antiviral activity using a cell-based method, we tested the cytotoxicity of GQDs on Madin–Darby canine kidney (MDCK) cells (Fig. 3a). The cells were exposed to GQDs for 24 h in growth media, stained by crystal violet, and washed to remove dead cells, and absorbance after lysis was measured. Notably, when the amount of GQDs exceeded 2.5 mg mL^{-1}, it induced severe cell death. In contrast, when the amount of GQDs was less than 1.25 mg mL^{-1}, no cytotoxicity was observed. Accordingly, 1.25 mg mL^{-1} was decided to be the limit concentration for our further cell-based investigation. The CC_{50} (50% cytotoxic concentration) value was calculated to be 2.18 mg mL^{-1}.

As we identified that virucidal mode of-action is independent of strain specificity, plaque forming reduction assay was assessed against various subtypes of influenza A virus, namely, A/Puerto Rico/8/34 (H1N1), A/X-31 (H3N2), A/aquatic bird/

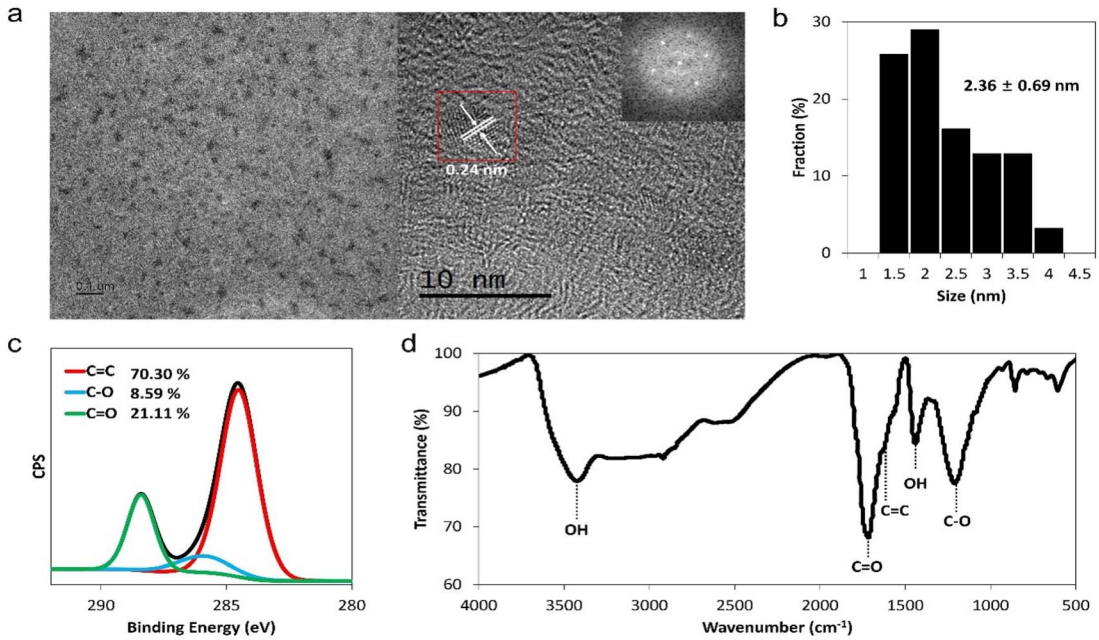

Fig. 1 Characteristics of GQDs. (a) TEM images and fast Fourier transform pattern of GQDs (inner box). (b) Size distribution of GQDs. (c) XPS C 1s spectra and (d) FT-IR spectra of GQDs.

Korea/w81/05 (H5N2), and A/Philippine/2/82 (H3N2) (Fig. 3b). GQDs completely inhibited all tested viruses at $\approx$1 mg mL^{-1}. The IC_{50} values for PR8 and X31 were 0.043 and 0.231 mg mL^{-1}, respectively, and those for aquatic bird and Philippine were expected to be 0.007 and 0.003 mg mL^{-1}, respectively. Time-of-addition assay results indicated that GQDs inhibited viral infection in the post-treatment scheme, exhibiting an IC_{50} value of 0.06 mg mL^{-1} (Fig. S5 and S6†). However, the pre-treatment of GQDs on cells did not suppress viral infection. These results demonstrated the therapeutic potential of GQDs against influenza infection. Moreover, since the disruption of virus was not related to the subtypes of viral proteins, such as hemagglutinin

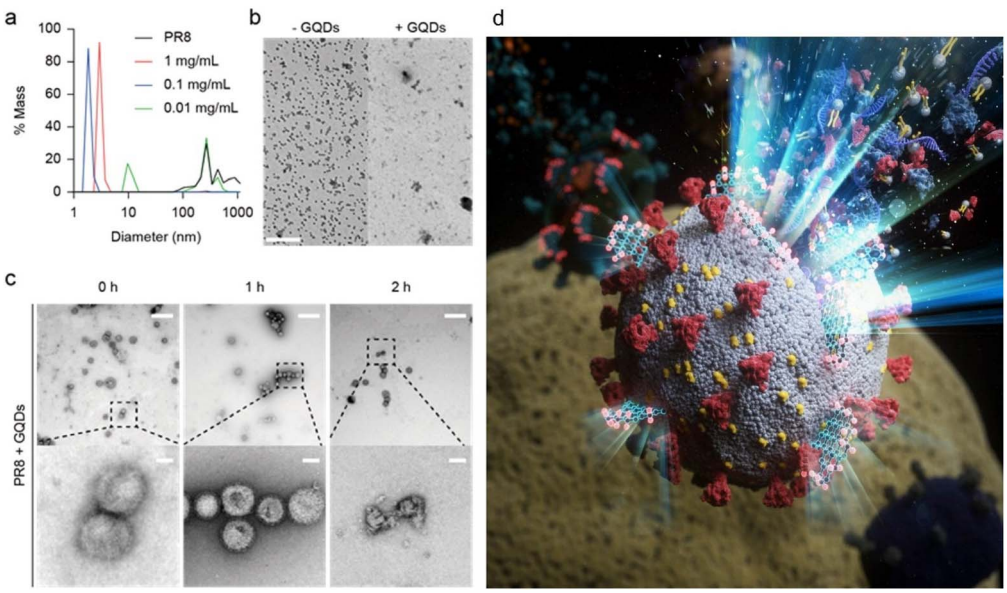

Fig. 2 Virucidal effect of GQDs on A/PR/8/34 virus. (a) Disruption of PR8 by GQDs measured by DLS. (b) TEM images of viruses in the absence and presence of GQDs (scale bar = 2 μm). (c) Time-dependent disruption of virions by GQDs observed under 0.05 mg mL^{-1} GQD treatment. At the mentioned time points of incubation, the virus-GQDs mixture was fixed by 4% formaldehyde, negatively stained, and imaged by TEM (scale bar = 500 nm for upper lane, 50 nm for bottom lane). (d) An illustration, corresponding to the TEM images in (c), representing the rupture of viral membranes on treatment with GQDs.

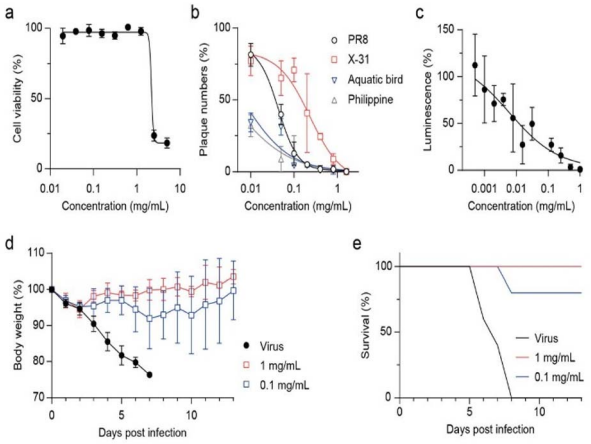

Fig. 3 Inhibitory activity on various strains of virus by GQDs. (a) Cell viability of GQDs measured in MDCK cells using crystal violet staining. (b) Anti-influenza effect of GQDs evaluated against several influenza A viruses. Each virus was treated with GQDs for 1 h at RT prior to infection. (c) Inhibitory effect on SARS-CoV-2 pseudoviruses (1.0×10^4 RLU mL^{-1}) determined in HEK293T cells expressing ACE2/TMPRSS2. (d and e) *In vivo* virucidal efficacy of GQDs against H1N1 infection. Body weight (d) and survival rate (e) monitored for 13 days post-infection ($n = 5$ per group).

and neuraminidase, GQDs demonstrated great potential as antiviral agents with broad-spectrum antiviral activity.

We further investigated the antiviral potential of GQDs against SARS-CoV-2 pseudoviruses (Fig. 3c and S7†). SARS-CoV-2 pseudoviruses (1.0×10^4 RLU mL^{-1}) were incubated with serially diluted GQDs (2-fold from 1 mg mL^{-1}) for 1 h at RT. HEK293T cells expressing human ACE2 and TMPRSS2 (293T-ACE2/TMPRSS2) were infected with the mixture, and luciferase activity was measured after incubation for 72 h at 37 °C under 5% CO_2. GQDs suppressed the infection of pseudoviruses with an IC_{50} value of 0.006 mg mL^{-1}. Since the cells expressed both ACE2 and TMPRSS2, this result suggested that disruption of virus by GQDs inhibited not only the receptor-mediated endocytosis but also the direct entry through the TMPRSS2-mediated activation of S proteins. In addition, we confirmed that GQDs suppressed the infection of the recombinant human adenovirus type 5 expressing enhanced green fluorescent protein (EGFP) (Fig. S8†).

In three different antiviral experiments against various viruses, including influenza A, adenovirus type 5 and pseudotyped SARS-CoV-2, GQDs exhibited consistent levels of viral inhibition. These results indicate that GQDs can act against a wide range of viruses regardless of their protein types and subtypes. Although their activity is not based on a specific mechanism, our previous research demonstrated the disaggregation of α-syn fibrils through charge interactions between negatively charged GQDs and positively charged part of the fibrils, followed by thermodynamic disassembly.[27] In light of these findings, we suggest that negatively charged oxygen-containing functional groups on GQDs are targeted to interact with the positive charge on the surface of viral capsids, resulting in a virucidal effect. For enveloped viruses, it is well known that the amphiphilicity of nanoparticles promotes the interaction with the viral lipid bilayers, thereby exerting a virucidal effect, as shown by graphene derivatives.[43–47] In our results, GQDs were found to demonstrate a broad virucidal activity along with viral membrane rupture over time, which is similar to other amphiphilic virucidal peptides. However, unlike large graphene derivatives, GQDs show low cytotoxicity because the cell membrane damage caused by the penetration of GQDs is negligible for lipid bilayers with a large curvature.[48–52]

We investigated whether the virucidal activity of GQDs can inhibit viral infection *in vivo* (Fig. 3d and e). When GQD (0, 0.1, or 1.0 mg mL^{-1})-treated PR8 viruses were intranasally injected in seven-week-old BALB/c female mice, 0.1 mg mL^{-1} rescued 80% mice from lethal infection, whereas the infected mice without GQDs lost 25% of body weight and were sacrificed at 7 dpi. Furthermore, the loss of body weight rapidly recovered after 3 dpi under the 1.0 mg mL^{-1} GQD treatment, rescuing all infected mice from lethality. Thus, we confirmed that the antiviral activity of GQDs through virucidal mode of action successfully inhibited the *in vivo* infection of H1N1 influenza A virus.

2.4 Characterization of well-purified small and large GQD samples

We fractionated synthesized GQDs as GQD-S and GQD-L through dialysis using a dialysis bag of 3 kDa molecular weight for 3 days. The filtered GQDs (<3 kDa) and GQDs remained in the dialysis bag (>3 kDa) were named GQD-S and GQD-L, respectively. As can be seen in Fig. 4a, GQD-S has a greenish-blue fluorescence and GQD-L has an orange fluorescence. GQD-S and GQD-L showed strong fluorescence peaks at 480 nm and 560 nm respectively. These two peaks correspond to the fluorescence peaks observed in the aforementioned GQDs (Fig. 4a, b and S4†). GQD-S was smaller than GQD-L in

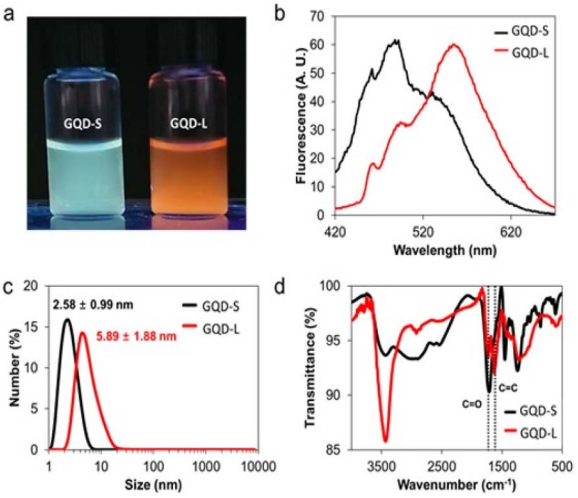

Fig. 4 GQD-S and GQD-L characterization. (a) Fluorescence images of GQD-S and GQD-L under 365 nm UV light. (b) Emission spectra of GQD-S and GQD-L at 365 nm excitation. (c) Hydrodynamic size distribution. (d) FT-IR spectra.

hydrodynamic size (Fig. 4c). Purified GQD-S and GQD-L were analyzed using FT-IR, XPS, and EA for identifying the functional groups and the carbon to oxygen ratio. In the FT-IR spectra, the ratio of peaks at 1620 cm^{-1} (C=C sp^2 carbon bonds) to peaks at 1720 cm^{-1} (C=O carboxylic acid) were ~0.51 and 1.23 in GQD-S and GQD-L, respectively (Fig. 4d). Moreover, through elemental analysis, we found that the C/O ratio of GQD-S was 0.808 and that of GQD-L was 1.317. These results indicate that GQD-S is more hydrophilic than GQD-L (Table S2†). This is due to GQD-S, being smaller than GQD-L, having more edge surface, more functional groups, and higher hydrophilicity.

2.5 Size-dependent hydrophilicity of GQDs and its influence on antiviral potency against enveloped viruses

Antiviral activity of the well-refined GQD-S and GQD-L were evaluated *in vitro* and *in vivo* (Fig. 5). Both GQDs showed no toxicity on MDCK cells at 5 mg mL^{-1} (Fig. 5a). Plaque reduction assay showed that GQD-S and GQD-L inhibited viral infection by influenza A and B viruses (Fig. 5b and c). IC_{50} values of GQD-S against A/PR8, A/X31, and A/Sydney were 0.098, 0.440, and 0.016 mg mL^{-1}, respectively. GQD-L, which was the larger and more hydrophobic GQD, exhibited IC_{50} values of 0.107, 0.772, and 0.270 μg mL^{-1} against A/PR8, A/X31, and A/Sydney, respectively. Owing to the virucidal mode of action of GQDs, B/Yamagata viruses were inhibited by these GQDs with size-dependent potency (IC_{50} values were 0.015 mg mL^{-1} and 0.270 μg mL^{-1} for GQD-S and -L, respectively). Interestingly, the inhibition of SARS-CoV-2 pseudoviruses by GQD-S and GQD-L differed significantly (Fig. 5d). At a concentration of 0.0625 mg mL^{-1}, GQD-S failed to inhibit SARS-CoV-2, whereas GQD-L completely suppressed viral infection *in vitro* (the IC_{50} value for GQD-L was 0.013 mg mL^{-1}). This gap in activity of GQD-S on influenza and pseudo SARS-CoV-2 viruses indicates that antiviral activity may depend on the membrane composition of the viral envelope.

Because influenza viruses are propagated in egg embryo and pseudoviruses are produced in 293T cells, their lipid components are different from each other, and they are expected to showcase varied antiviral potency.[53,54] Notably, GQD-L overcame this difference with considerable efficacy through its amphipathicity. This is owing to the large size of GQD-L, which manifests high hydrophobicity and concurrently acts as a more effective surfactant.[55,56] *In vivo* results against A/PR8 demonstrated that size-dependent virucidal activity of GQD-S and GQD-L acted effectively in the mouse model (Fig. 5e–g). At a high dose (1 mg mL^{-1}), both GQDs completely removed infectivity in all mice with 100% recovery of body weight (Fig. 5e and g). The antiviral activity was remarkably different at 0.1 mg mL^{-1} (Fig. 5f and g). Although 40% of the mice in the GQD-S-treated group survived 2 days longer than the negative controls, none of them recovered from infection. In contrast, the GQD-L-treated group showed 80% of survival rate at 13 dpi and fully restored their body weight loss.

3. Method

3.1 Pseudotyped SARS-CoV-2 virus

SARS-CoV-2 pseudoviruses expressing S-glycoproteins and a defective HIV-1 genome encoding luciferase were established. Supernatants containing SARS-CoV-2 pseudovirus were collected 48 h after transfection and utilized in the single-cycle infection of ACE2- and TMPRSS2-transfected 293T cells (293T ACE2/TMPRSS2). Serially diluted GQDs were incubated with 1×10^4 RLU mL^{-1} of SARS-CoV-2 pseudovirus for 1 h at room temperature prior to cell infection. The medium was replaced with a fresh medium 48 h later and incubated for 24 h.

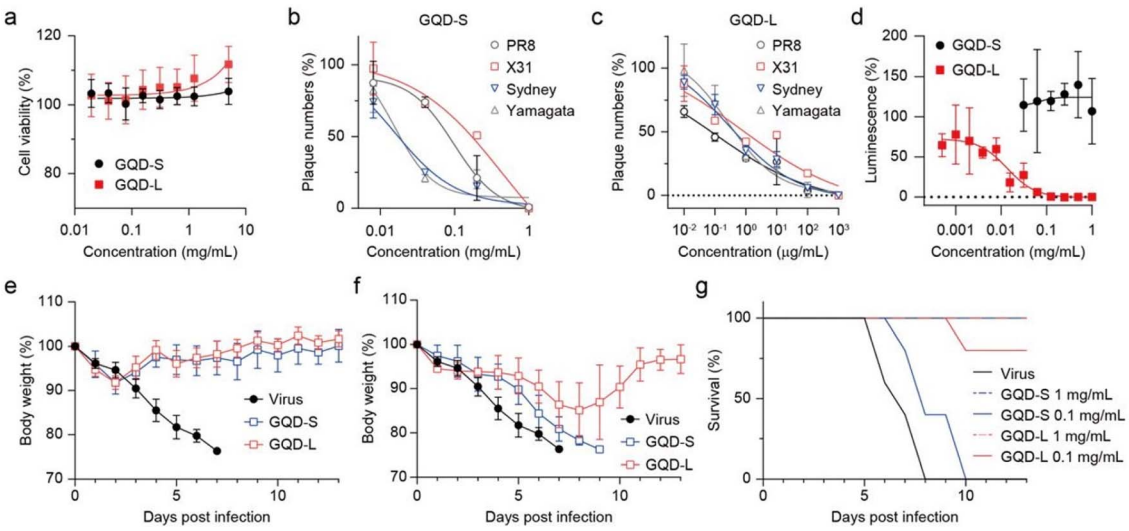

Fig. 5 Inhibitory activity on various strains of virus by GQD-S and GQD-L. (a) Cell viability of GQDs measured in MDCK cells. Anti-influenza effects of GQD-S (b) and GQD-L (c) evaluated against influenza A and B viruses using a plaque-forming reduction assay. (d) Inhibitory effect on SARS-CoV-2 pseudovirus (1.0×10^4 RLU mL^{-1}) determined in HEK293T cells expressing ACE2/TMPRSS2. (e–g) *In vivo* virucidal efficacy of GQD-S and GQD-L against H1N1 infection. Body weight ((e) using 1 mg mL^{-1} of GQDs, (f) using 0.1 mg mL^{-1} of GQDs) and survival rate (g) monitored for 13 days post-infection ($n = 5$ per group).

Luciferase activity of infected cells was measured as per the manufacturer's instructions (Promega, Madison, Wisconsin, USA).

3.2 Animals

Seven-week-old female BALB/c mice (Koatech, Inc., Pyeongtaek, Korea) were housed at five per cage with access to food and water ad libitum. The mice were intranasally infected with four-fold 50% lethal doses (LD_{50}) of A/PR/8/34 H1N1 virus or GQD-incubated virus, or they were mock-infected. Body weight and survival rate were monitored for 13 days post-infection. When a mouse lost 25% of its initial body weight, it was considered dead and humanely killed. All animal procedures were performed in accordance with the Guidelines for Care and Use of Laboratory Animals of Sungkyunkwan University, and experiments were approved by the Institutional Animal Care and Use Committee of Sungkyunkwan University (IACUC number: SKKUIACUC2021-05-25-1).

4. Conclusions

We investigated the antiviral activity of GQDs to be used as universal agents against viruses, regardless of the viral strain. In this study, we demonstrate that GQDs are capable of inhibiting viral infection in cellular and animal models with broad virucidal effects through direct interaction with viral membranes. Notably, irreversible *in vitro* inhibition was effective against a wide range of viruses, including enveloped viruses such as influenza and pseudotyped SARS-CoV-2 and even non-enveloped adenovirus.

The comparative analysis of GQD-S and GQD-L highlighted the critical role of size and hydrophilicity control in determining antiviral potency. This insight provides valuable guidance for the future design and optimization of GQD-based antiviral therapies. The observed differences in efficacy between GQD-S and GQD-L underscored the importance of fine-tuning these parameters to enhance the antiviral performance.

These results suggest the potential of GQDs to open new pathways to fight against pandemic diseases by offering a rapid and adaptable countermeasure against repeatedly occurring viral diseases. In particular, the unique properties of GQDs, including the size-dependent and hydrophilicity-controlled antiviral activities, would provide alternative strategies to fight the broad-spectrum of viral threats.

Data availability

The data supporting this article have been included as part of the ESI.†

Author contributions

Y. J., J. H., H. C. and M. A. conceptualized and conducted the experiments, validated the data, and contributed to writing. J. H. L. and J. S. contributed to materials synthesis and analysis of this work. J. H. Y. and D. K. assisted in antiviral analysis. D. H. K., B. H. H. and M. A. conceived and supervised the project.

Conflicts of interest

There are no conflicts to declare.

Acknowledgements

This work was supported by the National Research Foundation of Korea (NRF) grants funded by the Korea Government (MIST) (No. 2017R1A6A1A03015642, 2020R1A2C2101964, 2022M3E5F1081330, 2022R1A4A5034046 and RS-2021-NF000507).

Notes and references

1 L. A. Reperant and A. D. M. E. Osterhaus, *Vaccine*, 2017, **35**, 4470–4474.
2 P. R. Saunders-Hastings and D. Krewski, *Pathogens*, 2016, **5**, 66.
3 N. D. Wolfe, C. P. Dunavan and J. Diamond, *Nature*, 2007, **447**, 279–283.
4 B. K. Yoon, W.-Y. Jeon, T. N. Sut, N.-J. Cho and J. A. Jackman, *ACS Nano*, 2021, **15**, 125–148.
5 W. C. Koff, D. R. Burton, P. R. Johnson, B. D. Walker, C. R. King, G. J. Nabel, R. Ahmed, M. K. Bhan and S. A. Plotkin, *Science*, 2013, **340**, 1232910.
6 J. Wise, *BMJ*, 2021, **372**, n359.
7 P. Carravilla, A. Cruz, I. Martin-Ugarte, I. R. Oar-Arteta, J. Torralba, B. Apellaniz, J. Pérez-Gil, J. Requejo-Isidro, N. Huarte and J. L. Nieva, *Biophys. J.*, 2017, **113**, 1301–1310.
8 Q. Li, Z. Zhao, D. Zhou, Y. Chen, W. Hong, L. Cao, J. Yang, Y. Zhang, W. Shi, Z. Cao, Y. Wu, H. Yan and W. Li, *Peptides*, 2011, **32**, 1518–1525.
9 Y. Jung, B. Kong, S. Moon, S.-H. Yu, J. Chung, C. Ban, W.-J. Chung, S.-G. Kim and D.-H. Kweon, *Biochem. Biophys. Res. Commun.*, 2019, **517**, 507–512.
10 P. Innocenzi and L. Stagi, *Chem. Sci.*, 2020, **11**, 6606–6622.
11 V. Cagno, P. Andreozzi, M. D'Alicarnasso, P. Jacob Silva, M. Mueller, M. Galloux, R. Le Goffic, S. T. Jones, M. Vallino, J. Hodek, J. Weber, S. Sen, E.-R. Janeček, A. Bekdemir, B. Sanavio, C. Martinelli, M. Donalisio, M.-A. Rameix Welti, J.-F. Eleouet, Y. Han, L. Kaiser, L. Vukovic, C. Tapparel, P. Král, S. Krol, D. Lembo and F. Stellacci, *Nat. Mater.*, 2018, **17**, 195–203.
12 V. Cagno, M. Gasbarri, C. Medaglia, D. Gomes, S. Clement, F. Stellacci and C. Tapparel, *Antimicrob. Agents Chemother.*, 2020, **64**, e02001.
13 A. M. Chamoun, K. Chockalingam, M. Bobardt, R. Simeon, J. Chang, P. Gallay and Z. Chen, *Antimicrob. Agents Chemother.*, 2012, **56**, 672–681.
14 B. Kong, S. Moon, Y. Kim, P. Heo, Y. Jung, S.-H. Yu, J. Chung, C. Ban, Y. H. Kim, P. Kim, B. J. Hwang, W.-J. Chung, Y.-K. Shin, B. L. Seong and D.-H. Kweon, *Nat. Commun.*, 2019, **10**, 185.

15 T. Du, J. Lu, L. Liu, N. Dong, L. Fang, S. Xiao and H. Han, *ACS Appl. Bio Mater.*, 2018, **1**, 1286–1293.
16 S. Ye, K. Shao, Z. Li, N. Guo, Y. Zuo, Q. Li, Z. Lu, L. Chen, Q. He and H. Han, *ACS Appl. Mater. Interfaces*, 2015, **7**, 21571–21579.
17 Y.-N. Chen, Y.-H. Hsueh, C.-T. Hsieh, D.-Y. Tzou and P.-L. Chang, *Int. J. Environ. Res. Public Health*, 2016, **13**, 430.
18 T. Du, J. Liang, N. Dong, L. Liu, L. Fang, S. Xiao and H. Han, *Carbon*, 2016, **110**, 278–285.
19 A. Łoczechin, K. Séron, A. Barras, E. Giovanelli, S. Belouzard, Y.-T. Chen, N. Metzler-Nolte, R. Boukherroub, J. Dubuisson and S. Szunerits, *ACS Appl. Mater. Interfaces*, 2019, **11**, 42964–42974.
20 D. Iannazzo, A. Pistone, S. Ferro, L. De Luca, A. M. Monforte, R. Romeo, M. R. Buemi and C. Pannecouque, *Bioconjugate Chem.*, 2018, **29**, 3084–3093.
21 M. Sametband, I. Kalt, A. Gedanken and R. Sarid, *ACS Appl. Mater. Interfaces*, 2014, **6**, 1228–1235.
22 C. J. Lin, L. Chang, H. W. Chu, H. J. Lin, P. C. Chang, R. Y. L. Wang, B. Unnikrishnan, J. Y. Mao, S. Y. Chen and C. C. Huang, *Small*, 2019, **15**, e1902641.
23 D. Ting, N. Dong, L. Fang, J. Lu, J. Bi, S. Xiao and H. Han, *ACS Appl. Nano Mater.*, 2018, **1**, 5451–5459.
24 H.-T. Huang, H.-J. Lin, H.-J. Huang, C.-C. Huang, J. H.-Y. Lin and L.-L. Chen, *Sci. Rep.*, 2020, **10**, 7343.
25 Z. Song, X. Wang, G. Zhu, Q. Nian, H. Zhou, D. Yang, C. Qin and R. Tang, *Small*, 2015, **11**, 1171–1176.
26 I. Kang, J. M. Yoo, D. Kim, J. Kim, M. K. Cho, S.-E. Lee, D. J. Kim, B.-C. Lee, J. Y. Lee, J.-J. Kim, N. Shin, S. W. Choi, Y.-H. Lee, H. S. Ko, S. Shin, B. H. Hong and K.-S. Kang, *Nano Lett.*, 2021, **21**, 2339–2346.
27 D. Kim, J. M. Yoo, H. Hwang, J. Lee, S. H. Lee, S. P. Yun, M. J. Park, M. Lee, S. Choi, S. H. Kwon, S. Lee, S.-H. Kwon, S. Kim, Y. J. Park, M. Kinoshita, Y.-H. Lee, S. Shin, S. R. Paik, S. J. Lee, S. Lee, B. H. Hong and H. S. Ko, *Nat. Nanotechnol.*, 2018, **13**, 812–818.
28 Y. Chong, Y. Ma, H. Shen, X. Tu, X. Zhou, J. Xu, J. Dai, S. Fan and Z. Zhang, *Biomaterials*, 2014, **35**, 5041–5048.
29 M. Nurunnabi, Z. Khatun, K. M. Huh, S. Y. Park, D. Y. Lee, K. J. Cho and Y.-k. Lee, *ACS Nano*, 2013, **7**, 6858–6867.
30 J. Li, X. Wang, K.-C. Mei, C. H. Chang, J. Jiang, X. Liu, Q. Liu, L. M. Guiney, M. C. Hersam, Y.-P. Liao, H. Meng and T. Xia, *Nano Today*, 2021, **37**, 101061.
31 B.-C. Lee, J. Y. Lee, J. Kim, J. M. Yoo, I. Kang, J.-J. Kim, N. Shin, D. J. Kim, S. W. Choi, D. Kim, B. H. Hong and K.-S. Kang, *Sci. Adv.*, 2020, **6**, eaaz2630.
32 B.-C. Lee, J. Y. Lee, J. Kim, N. Shin, J. M. Yoo, I. Kang, J.-J. Kim, S.-E. Lee, D. Kim, S. W. Choi, B. H. Hong and K.-S. Kang, *2D Mater.*, 2021, **8**, 025036.
33 D. Zhang, Z. Zhang, Y. Wu, K. Fu, Y. Chen, W. Li and M. Chu, *Biomaterials*, 2019, **194**, 215–232.
34 S. Wang, I. S. Cole and Q. Li, *RSC Adv.*, 2016, **6**, 89867–89878.
35 L. Ou, B. Song, H. Liang, J. Liu, X. Feng, B. Deng, T. Sun and L. Shao, *Part. Fibre Toxicol.*, 2016, **13**, 57.
36 C.-T. Hsieh, S. Gu, Y. A. Gandomi, C.-C. Fu, P.-Y. Sung, R.-S. Juang and C.-C. Chen, *J. Colloid Interface Sci.*, 2023, **630**, 1–10.
37 D. Iannazzo, S. V. Giofrè, C. Espro and C. Celesti, *Expert Opin. Drug Delivery*, 2024, **21**, 751–766.
38 F. Liu, Y. Sun, Y. Zheng, N. Tang, M. Li, W. Zhong and Y. Du, *RSC Adv.*, 2015, **5**, 103428–103432.
39 T. Gao, X. Wang, L.-Y. Yang, H. He, X.-X. Ba, J. Zhao, F.-L. Jiang and Y. Liu, *ACS Appl. Mater. Interfaces*, 2017, **9**, 24846–24856.
40 S. Khan, A. Sharma, S. Ghoshal, S. Jain, M. K. Hazra and C. K. Nandi, *Chem. Sci.*, 2018, **9**, 175–180.
41 Y. Li, Y. Hu, Y. Zhao, G. Shi, L. Deng, Y. Hou and L. Qu, *Adv. Mater.*, 2011, **23**, 776–780.
42 F. Ehrat, S. Bhattacharyya, J. Schneider, A. Löf, R. Wyrwich, A. L. Rogach, J. K. Stolarczyk, A. S. Urban and J. Feldmann, *Nano Lett.*, 2017, **17**, 7710–7716.
43 Y. Li, H. Yuan, A. von dem Bussche, M. Creighton, R. H. Hurt, A. B. Kane and H. Gao, *Proc. Natl. Acad. Sci. U. S. A.*, 2013, **110**, 12295–12300.
44 J. Chen, G. Zhou, L. Chen, Y. Wang, X. Wang and S. Zeng, *J. Phys. Chem. C*, 2016, **120**, 6225–6231.
45 X. Zou, L. Zhang, Z. Wang and Y. Luo, *J. Am. Chem. Soc.*, 2016, **138**, 2064–2077.
46 X. Zhang, F. Cao, L. Wu and X. Jiang, *Langmuir*, 2019, **35**, 14098–14107.
47 L. Wu, L. Zeng and X. Jiang, *J. Am. Chem. Soc.*, 2015, **137**, 10052–10055.
48 L. Liang, Z. Kong, Z. Kang, H. Wang, L. Zhang and J.-W. Shen, *ACS Biomater. Sci. Eng.*, 2016, **2**, 1983–1991.
49 J. A. Jackman, G. H. Zan, V. P. Zhdanov and N.-J. Cho, *J. Phys. Chem. B*, 2013, **117**, 16117–16128.
50 J. A. Jackman, R. Saravanan, Y. Zhang, S. R. Tabaei and N.-J. Cho, *Small*, 2015, **11**, 2372–2379.
51 D. Koller and K. Lohner, *Biochim. Biophys. Acta, Biomembr.*, 2014, **1838**, 2250–2259.
52 S. R. Tabaei, M. Rabe, V. P. Zhdanov, N.-J. Cho and F. Höök, *Nano Lett.*, 2012, **12**, 5719–5725.
53 P. T. Ivanova, D. S. Myers, S. B. Milne, J. L. McClaren, P. G. Thomas and H. A. Brown, *ACS Infect. Dis.*, 2015, **1**, 435–442.
54 S. E. Farley, J. E. Kyle, H. C. Leier, L. M. Bramer, J. B. Weinstein, T. A. Bates, J.-Y. Lee, T. O. Metz, C. Schultz and F. G. Tafesse, *Nat. Commun.*, 2022, **13**, 3487.
55 M. Simon, M. Veit, K. Osterrieder and M. Gradzielski, *Curr. Opin. Colloid Interface Sci.*, 2021, **55**, 101479.
56 P.-Z. Zhang, F.-F. Jiao, Z.-X. Xie, Z. Kong, W. Hu, J.-W. Shen and L.-J. Liang, *Mater. Adv.*, 2022, **3**, 6161–6170.